Title

A Rapid and Low-Cost Pathogen Detection Platform by Using a Molecular Agglutination Assay

Journal

ACS Central Science, 4(11)

ISSN

2374-7943

Authors

Wu, Tsung-Feng
Chen, Yu-Chen
Wang, Wei-Chung
et al.

Publication Date

2018-11-28

DOI

10.1021/acscentsci.8b00447

Peer reviewed

ACS central science

Research Article

Cite This: ACS Cent. Sci. 2018, 4, 1485−1494

http://pubs.acs.org/journal/acscii

A Rapid and Low-Cost Pathogen Detection Platform by Using a Molecular Agglutination Assay

Tsung-Feng Wu,*[,†,#] Yu-Chen Chen,[†,#] Wei-Chung Wang,[†] Yen-Chi Fang,[†] Scott Fukuoka,[‡] David T. Pride,[§] and On Shun Pak*[,⊥]

[†]VOR, Inc., Atkinson Hall #1412, 9500 Gilman Drive, La Jolla, California 92093, United States

[‡]Department of Bioengineering, Santa Clara University, 500 El Camino Real, Santa Clara, California 95053, United States

[⊥]Department of Mechanical Engineering, Santa Clara University, 500 El Camino Real, Santa Clara, California 95053, United States

[§]Department of Pathology, University of California at San Diego, 9500 Gilman Drive #0612, La Jolla, California 92093, United States

Supporting Information

ABSTRACT: Rapid and low-cost pathogen diagnostic approaches are critical for clinical decision-making procedures. Cultivating bacteria often takes days to identify pathogens and provide antimicrobial susceptibilities. The delay in diagnosis may result in compromised treatment and inappropriate antibiotic use. Over the past decades, molecular-based techniques have significantly shortened pathogen identification turnaround time with high accuracy. However, these assays often use complex fluorescent labeling and nucleic acid amplification processes, which limit their use in resource-limited settings. In this work, we demonstrate a wash-free molecular agglutination assay with a straightforward mixing and incubation step that significantly simplifies procedures of molecular testing. By targeting the 16S rRNA gene of pathogens, we perform a rapid pathogen identification within 30 min on a dark-field imaging microfluidic cytometry platform. The dark-field images with low background noise can be obtained using a narrow beam scanning technique with off-the-shelf complementary metal oxide semiconductor (CMOS) imagers such as smartphone cameras. We utilize a machine learning algorithm to deconvolute topological features of agglutinated clusters and thus quantify the abundance of bacteria. Consequently, we unambiguously distinguish *Escherichia coli* positive from other *E. coli* negative among 50 clinical urinary tract infection samples with 96% sensitivity and 100% specificity. Furthermore, we also apply this quantitative detection approach to achieve rapid antimicrobial susceptibility testing within 3 h. This work exhibits easy-to-use protocols, high sensitivity, and short turnaround time for point-of-care testing uses.

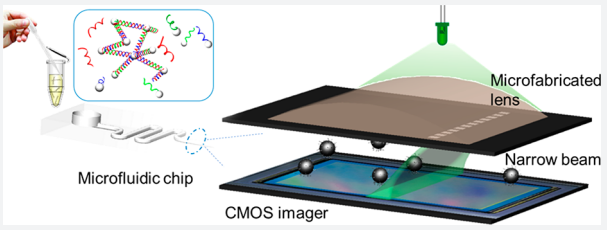

There has been a strong need for rapid infectious disease diagnostics to identify causative pathogens and expedite treatment strategies. Bacterial culture generally take days, resulting in delayed treatment and inappropriate antibiotic use.[1] Urinary tract infections (UTIs) are one of the most common bacterial infections, accounting for more than 8 million hospital visits in the United States, where 84% of occurrences are in women.[2,3] UTIs also are the most common cause of healthcare-associated infections in the United States because 15−25% hospitalized patients receive urinary catheters during their hospital stay.[4,5] UTIs cost the healthcare system more than 3 billion dollars annually due to extended hospital stays, disability, and antibiotics usage.[6−8]

In clinical guidelines, empirical antibiotic treatment is recommended as firsthand UTI treatment based on the most frequent pathogens identified and local patterns of antimicrobial resistance until causative bacteria and their antibiotic susceptibilities are identified.[9] Thus, inappropriate use of antibiotics may lead to growth of resistant bacteria, which decreases the efficacy of existing antibiotics and limits available treatment options.[10] Antimicrobial resistance has become one of the most challenging public health issues today. To this end, a rapid UTI diagnostic platform can offer treatment guidance by incorporating antimicrobial susceptibility testing (AST).[11]

The deployment of rapid diagnostic methods at point-of-care testing (POCT) levels is essential to improving healthcare quality and guiding clinical decisions, especially in resource-limited settings.[12,13] Over the past few decades, molecular diagnostic technologies such as polymerase chain reaction have been applied for pathogen identification. The nucleic acid amplification tests (NAATs) offer a powerful technique for a rapid pathogen identification. However, the NAAT approaches have shortcomings such as complex sample preparation, high equipment and reagent costs, amplification of nonviable organisms, and necessity of qualified technicians among others.[14,15] The lack of sufficient lab instruments such as water baths, shakers, thermal cyclers, etc. discourages the use

Received: July 9, 2018
Published: November 5, 2018

DOI: 10.1021/acscentsci.8b00447
ACS Cent. Sci. 2018, 4, 1485−1494

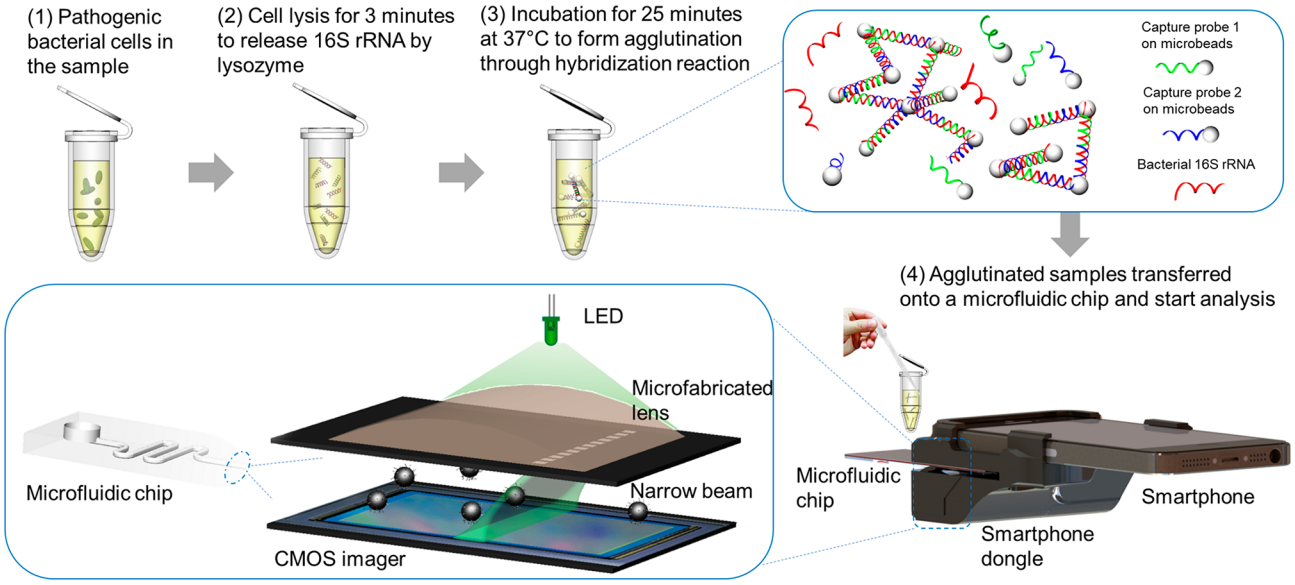

Figure 1. Schematic molecular agglutination assay protocol and detection setup. (1) Bacterial cells suspended in the solution. (2) Cell lysis by lysozyme to release target 16S rRNA from bacterial cells at room temperature. (3) Incubation of 16S rRNA with probe-coated microparticles at 37 °C in the buffer solution, where a pair of probes bind with target 16S rRNA sequences to form agglutination through hybridization. (4) Agglutinated cluster in the solution transferred to a microfluidic chip and analyzed by a dark-field imaging flow cytometer implemented on the smartphone, where a smartphone dongle consists of a microfabricated lens glass slide, an inverse microlens, and an LED. The overall turnaround time takes less than 30 min from the sample to analyzed results.

of NAATs for clinical end-users in resource-limited settings. Although the development of POCT diagnostics on portable electronics have shown promising results,[16,17] the miniaturization of NAAT techniques and their deployment in POCT settings remain challenging due to system integration and testing reliability. Thus, few technologies can deliver a "sample-in, answer-out" approach for operation and meet POCT requirements in practice.

In this paper, we propose a low-cost microfluidic imaging flow cytometry platform for rapid UTI diagnostics. The platform utilizes the narrow beam scanning (NBS) technique with off-the-shelf complementary metal-oxide-semiconductor (CMOS) imagers to collect images from molecular agglutination bioassays.[18,19] The agglutination assay is a simple approach to produce signals detected by various biosensors.[20−23] These bioassays have mostly been demonstrated by means of antibody-coated microparticles for detection of biomarkers or bacteria.[24,25] Recently, the advancement of molecular diagnostics allows an innovative agglutination format through nucleic acid hybridization to detect amplicons of polymerase chain reaction (PCR) or other nucleic acid targets.[22,26−28] We harness the molecular approach that immobilizes a pair of oligonucleotide probes on microparticles, respectively, followed by agglutination formation against target bacterial nucleic acid through a hybridization reaction. Because there are more than 10 000 copies of 16S ribosomal ribonucleic acid (rRNA) per bacterial cell,[29] this high abundance not only allows us to circumvent drawbacks of nucleic acid amplification, but also ensures high sensitivity against target bacteria. The probes are designed to be complementary to specific 16S rRNA of target UTI bacteria. Once probes on microparticles hybridize with target 16S rRNA, the scattered light of agglutinated clusters will be imaged on the CMOS imagers by the NBS technique. Different bacterial concentrations in the sample display distinct features of agglutination patterns. To assist the quantification of bacterial concentration from these agglutination patterns, we demonstrate the novel application of machine learning algorithms with image processing to analyze images of scattered light from agglutinated clusters. The quantitative outputs of our rapid and low-cost platform enable clinical pathogen diagnostics and antibiotics selection guidance via AST in POCT settings.

The use of molecular agglutination bioassays in our platform simplifies protocols and enables rapid pathogen identification. As a proof-of-concept for UTI diagnostics, we conduct our protocols and use a smartphone camera as the readout system. The major advantages of the proposed platform include: (1) bacterial identification with high sensitivity and specificity: utilize widely proven 16S rRNA detection to identify causative UTI bacteria directly,[30] (2) cost effectiveness: use fluorescent-free reagents and low-cost microparticles to reduce cost per test, (3) short turnaround time: conduct hybridization in the solution phase, facilitating agglutination formation, (4) one-pot protocol: mix lysate with probe-coated microparticles for direct detection without washing steps, and (5) quantitative detection: offer a rapid AST solution for clinical treatment guidance. Our preliminary results demonstrate a rapid detection protocol that can complete *Escherichia coli* (*E. coli*) detection with a limit of detection down to 10^2 colony-forming unit (CFU) per mL within 30 min. We also apply the same protocols to distinguish *E. coli* positive samples from 50 clinical samples, showing high clinical specificity. The growth-based dose−response testing can be completed within 3 h to clearly quantify bacterial level change, indicating the proposed platform holds potential for clinical treatment guidance.

RESULTS AND DISCUSSION

In this work, we blend the benefits of molecular testing and novel imaging techniques to design a rapid and low-cost pathogen detection platform. We improve upon molecular agglutination bioassays by quantifying the output in a low-cost

DOI: 10.1021/acscentsci.8b00447
ACS Cent. Sci. 2018, 4, 1485−1494

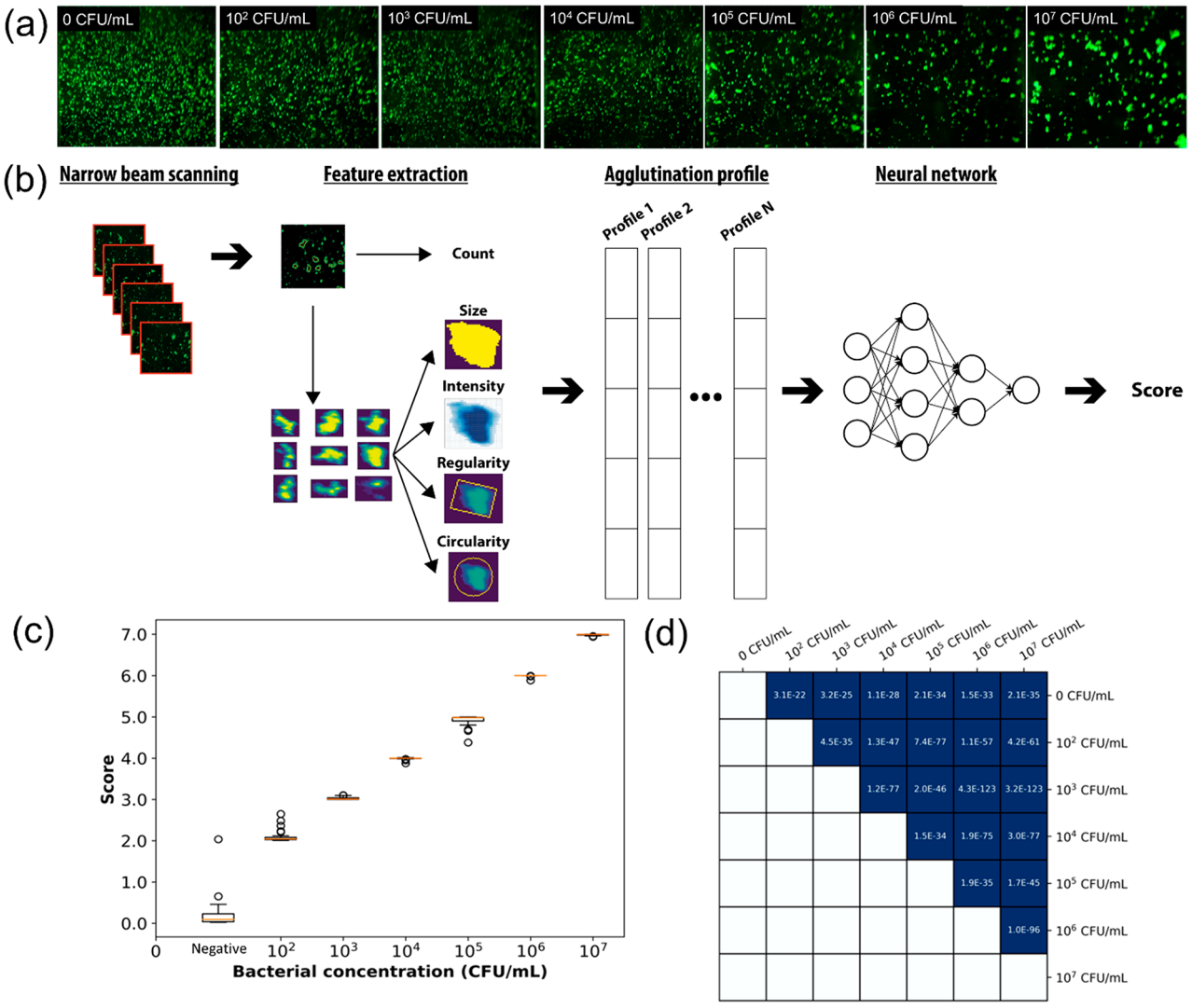

Figure 2. (a) Snapshot of agglutinated microparticles flowing through the microfluidic channel at each bacterial concentration. Images are recorded on an iPhone 5S. (b) Overview of a machine learning algorithm to train a neural network to score agglutinated patterns for quantification of bacterial levels. The count is an intrinsic feature to describe the number of agglutinated clusters. Besides, four agglutinated features are extracted using image process algorithms: (1) size, (2) scattered light intensity, (3) regularity, and (4) circularity. (c) Quantification of *E. coli* using the neural network. The line in orange represents the median of scores at bacterial concentration of 0, 10^2, 10^3, 10^4, 10^5, 10^6, and 10^7 CFU/mL. The upper and lower boundaries of the boxplot are determined by the first quantile (Q1), the third quantile (Q3), and interquartile range (IQR). The IQR equals Q3 − Q1. The lower boundary equals Q1 − 1.5*IQR and the upper boundary equals Q3 − 1.5*IQR. (d) The *p*-value for the pairwise comparison of score distribution at different bacterial concentrations using two sample Student's *t* test.

microfluidic imaging flow cytometry platform. The use of a microfluidic platform transports the agglutinated clusters in flow, which allows a sufficiently large number of images to be taken from the product of the agglutination assay for statistical analyses. The geometry of the microfluidic channel also allows agglutination clusters in the flow to be distributed within the depth of focus, which produces more clear images of the clusters for imaging processing. The microfluidic channels are fabricated using adhesive tapes coated with hydrophilic materials to drive fluid flow via a capillary effect, which eliminates the need for external pumps and hence reduces the cost and complexity of the overall system. The use of the NBS technique with off-the-shelf CMOS imagers facilitates point-of-care testing uses. Finally, we highlight the novel application of machine learning algorithms to improve the quantification of bacterial concentration from agglutination patterns in this work. We discuss each component of our platform in detail in the following sections.

Microfluidic Imaging Flow Cytometry Platform. The proposed microfluidic imaging flow cytometry platform for rapid pathogen identification is illustrated in Figure 1. As demonstrated in the previous work, a tilted narrow beam can be formed by the microfabricated lens, where a slit opening underlays near the edge of the microlens.[19] This titled beam produces scattered light from the objects of interest. We mix the bacterial lysate with probe-coated microparticles and flow the liquid mixture through the microfluidic channel. The refractive index difference between microparticles and medium generates scattered light, which can be readily detected by the CMOS imager. The narrow beam illuminates microparticles at a fixed incident angle so that the CMOS imager collects only the scattered light but not the primary beam, forming a dark-field imaging band with minimal background noise. Given the

DOI: 10.1021/acscentsci.8b00447
ACS Cent. Sci. 2018, 4, 1485−1494

30 frame per second (fps) recording rate of the iPhone 5S camera, the serpentine channel before the sensing window is designed to slow down the flow rate to capture discernible images. The latest CMOS imager with higher recording performance can further improve image quality for downstream analysis. The laser cutting process is used to engrave a microfluidic design on a light shielding film. The light shield film with double-sided adhesive is then sandwiched with hydrophilic films. Once the liquid sample is transferred onto the microfluidic device, capillary effects will spontaneously imbibe samples into the microchannel. Our platform does not require any external pumping mechanism, which reduces the overall costs and improves the ease of use in POCT settings.

A compact smartphone dongle is designed to integrate a green light-emitting diode (LED) as an illumination source, a microlens-embedded glass slide, and an optical lens. The optical lens is used to magnify the agglutinated clusters and enlarge the field of view, which can fully cover the entire dark-field imaging band.[31,32]

Molecular Agglutination Assay. Traditional clinical diagnosis based on agglutination assays relies on visual examination by naked eyes. However, the lack of sensitivity and subjective judgment by visual examination are potential pitfalls for decision-making. Here we adopt off-chip protocols for sample preparation and focus on demonstrating a POCT detection platform. As illustrated in Figure 1, bacteria are lysed to release target 16S rRNA. A pair of capture probes (EC1 and EC2) immobilized on magnetic microparticles, respectively, are mixed with the lysate. Each capture probe has a C12-linker between its oligonucleotides and biotinylated end to reduce steric hindrance during hybridization. The magnetic microparticles generally have better suspension and less self-aggregation, which is critical to our image processing algorithms. Upon addition of hybridization buffer, the presence of 16S rRNA and probe-coated microparticles will induce agglutination by the hybridization reaction. In our protocols, the hybridization occurs in the solution, where a faster reaction rate is expected due to elimination of inefficient diffusion processes.[33] We also notice that the high stringency buffer conditions have to be applied to avoid agglutination from nonspecific binding. Under the high salt concentrations, agglutination is observed within 5 min after adding the hybridization buffer even for nontarget bacteria. To prevent nonspecific agglutination, 1% bovine serum albumin (BSA) is a minimal amount in the hybridization buffer. The incubation temperature is set at 37 °C for 25 min. The microparticle numbers have to be experimentally tuned to achieve a desired limit of detection within a target dynamic range of the agglutination assay.[34,35] This is because when the binding capacity on microparticles is greater than target analyte, the linear detection performance can be obtained. Due to the clinical criteria of the UTI diagnosis being 10^5 CFU/mL,[36−38] the dynamic range of the present agglutination assay is designed to include bacterial concentration between 10^2 and 10^7 CFU/mL. In 100 μL of the final mixture, about $\sim 2.4 \times 10^7$ probe-coated microparticles are present to react with target rRNA to form agglutination. After hybridization, the mixture can be directly pipetted onto the microfluidic chip for analysis using the NBS technique. As a key feature, the strategy using two capture probes directed against the target sequence can be expanded to a generic principle for pathogen detection. Unlike other optical-based methods, such as fluorescent probes, our platform uses dark-field imaging to form images on low-cost CMOS imagers as a readout system. Using the agglutination format, we are able to conduct a "wash-free" assay. This microfluidic imaging flow cytometer platform holds the potential to deliver a ready-to-use POCT system. Another inherent advantage of our platform is the low cost per test and inexpensive readout system, which is critical to budget control of the healthcare ecosystem.

Quantitative Detection of *E. coli* by Agglutination Pattern. The present dark-field imaging flow cytometry platform exploits the agglutination pattern changes, which clearly captures agglutinated clusters on a two-dimensional plane, boosting the features on the agglutination pattern. In contrast to traditional fluorescent detection, the intensity of fluorescence is the only signal that can be detected for detection. As a result, great attention to the quality of fluorophore and quencher molecules and handling procedures is necessary.

To demonstrate our platform, we selected *E. coli*, the most common causative UTI pathogen, as the first target bacteria. Under the optimized hybridization conditions, we serially diluted cultured *E. coli* (JM109 strain) and conducted protocols to record images of the agglutination pattern at each bacterial level. In Figure 2a, we observe a concentration-dependent pattern using our approach with 5 orders of magnitude dynamic range. At a high concentration above 10^5 CFU/mL, the probe-coated microparticles can easily hybridize with target bacterial 16S rRNA sequences, leading to large agglutinated clusters and less unbound microparticles. On the other hand, when the target rRNA sequence exists in low abundance, most microparticles will remain unbound. We apply an image processing algorithm to identify pattern variables for bacterial level quantification.

A total of 39 500 images for agglutination patterns at bacterial concentration of 0, 10^2, 10^3, 10^4, 10^5, 10^6, and 10^7 CFU/mL were collected. Five agglutinated features were recognized to confer the maximum accuracy of quantification. As illustrated in Figure 2b, these features of each agglutinated cluster include (1) size, (2) scattered light intensity, (3) regularity, and (4) circularity. The *count* is a feature to describe the number of agglutinated clusters in each image. The features of agglutinated clusters from captured images could have large variance because the images are recorded in the continuous flow in the microfluidic channel. To reduce the impact from this variance in each frame, the accumulation of the features is conducted from every 50 frames to produce agglutination profiles. A total of 790 agglutination profiles were generated and learned by machine learning algorithms for quantification of the level of bacterial in the sample from the agglutination patterns.

As shown in Table 1, individual features from the agglutination profile do not correlate well with the concentration levels. For instance, the intensity of scattered

Table 1. Quantification Accuracy Using Individual Features from the Agglutination Profile

features	MSE	R^2
regularity	1.31	0.73
count	1.51	0.69
circularity	1.60	0.67
size	1.62	0.67
intensity	2.30	0.53

DOI: 10.1021/acscentsci.8b00447
ACS Cent. Sci. 2018, 4, 1485−1494

light shows a large mean squared error (MSE) of 2.30 and poor R^2 of 0.53. Although some particular features, such as Regularity, may perform discernible results at certain bacterial levels, the large coefficient of variation of measured features is found across different bacterial concentrations (Supporting Information, Figure S1). The results demonstrate that individual measures are insufficiently accurate for clinical purposes, suggesting a multidimensional analysis of the agglutination profile.

Multidimensional Profiles Boost Quantification Accuracy. Three different machine learning algorithms including linear regression, support vector machine (SVM), and neural network trained on the agglutination profile were further applied to increase accuracy.[39,40] As described in Materials and Methods, each machine learning algorithm learns features from the agglutination profile and produces a score. The performance was evaluated by MSE and R^2 in Table 2. The linear regression model outperforms the quantification accuracy using an individual agglutinated feature, but it still lacks the required sensitivity to differentiate bacterial concentration between 10^2 and 10^4 CFU/mL (Supporting Information, Figure S2). The SVM model shows improved performance; however, a wide score deviation at the bacterial concentration of 10^2, 10^4, and 10^7 CFU/mL makes precise quantification difficult (Supporting Information, Figure S3).

Table 2. Quantification Accuracy of Machine Learning Models on Validation Set

algorithms	MSE	R^2
neural network	0.02	0.99
SVM-RBF[a]	0.21	0.97
linear regression	0.90	0.85

[a]RBF: radial basis function kernel in SVM analysis.

Figure 2c shows the score generated by the neural network. The performance of neural network model on the validation set, consisting of 237 agglutination profiles, shows a low MSE of 0.03 and R^2 of 0.99. This model yields approximately 43-fold improvement on MSE and 26% improvement on R^2 comparing to Regularity, the individual feature with the best discernible results among the agglutination profiles. Moreover, the neural network model also outperforms the linear regression model with 30-fold improvement on MSE and the SVM model with 7-fold improvement on MSE. The results suggest that the activation function used in the neural network model greatly improves the quantification accuracy. The Student's t test was used to determine whether two score distributions are significantly different from each other. The pairwise comparison between score distributions for seven bacterial concentration levels of 0, 10^2, 10^3, 10^4, 10^5, 10^6, and 10^7 CFU/mL is shown in Figure 2d. We observe that the score distribution at one bacterial concentration level is statistically discernible from others with a small p-value less than 10^{-10}. The limit of detection (LOD) for the capture probe pairs targeting *E. coli* is 10^2 CFU/mL, defined by adding three standard deviations (SD) from the negative control mean (Supporting Information, Table S1). Machine learning algorithms trained on multidimensional agglutination profile can effectively quantify bacterial concentrations and produce high sensitivity, in which one-dimensional, intensity-based scattered light measurement and individual agglutinated features are not achievable by the agglutination assay (Supporting Information, Figure S4).

Clinical Validation: Specificity. The specificity of using the optimized agglutination assay is validated with clinical samples. We tested 50 clinical patient urine samples that were first examined in the hospital laboratory for microbiological analysis. According to the laboratory results, 25 samples were identified to be *E. coli* positive. Twenty-five samples are *E. coli* negative species (Supporting Information, Table S2). *E. coli* positive samples were cultured and concentration was calibrated to 10^6 CFU/mL. On the other hand, *E. coli* negative samples were tested at the concentration about 10^8 CFU/mL. These culturing and calibration steps were performed in this proof-of-concept implementation to demonstrate the consistency of our quantitative results using calibrated samples of live bacteria. These steps will not be necessary in an actual test for UTI diagnosis. Images were analyzed with an established machine learning model, with a cutoff score of 5, which corresponds to the clinical threshold concentration of 10^5 CFU/mL. Figure 3 shows that even highly concentrated *E. coli* negative samples do not produce scores above 5, the clinical criteria for UTI diagnosis. The *E. coli* positive samples have the mean score of 6.58 with standard deviation (SD) of 0.75, whereas the *E. coli* negative samples have the mean score of 2.38 with SD of 1.27. The Student's t test shows that the score distributions between *E. coli* positive and negative samples is statistically different with a p-value of 4.06×10^{-10}. The low yet quantifiable levels of agglutination in *E. coli* negative samples are attributed to minor cross reactivity against *E. coli* nucleotide probes. Combining the NBS technique and machine learning algorithms, the molecular agglutination assay demonstrated sensitivity of 96% and specificity of 100% for pathogen identification. More importantly, this approach significantly reduces turnaround time from 24 h to 30 min and simplifies assay procedures. As a remark, an actual

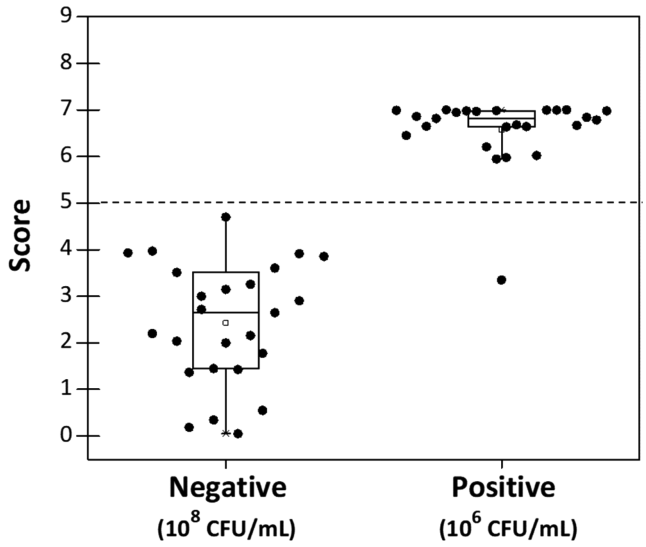

Figure 3. Clinical specificity validation with 50 clinical pathogens using *E. coli* probes. The sample classification results on horizontal axis results are examined from clinical laboratory test. The score on the vertical axis is obtained by the established machine learning algorithms. *E. coli* positive samples (24 out of 25) shows 96% detection sensitivity. All *E. coli* negative samples at 10^8 CFU/mL (100-fold higher than positive samples) are below the threshold value, which indicates 100% detection specificity and matches clinical microbiology results.

DOI: 10.1021/acscentsci.8b00447
ACS Cent. Sci. 2018, 4, 1485−1494

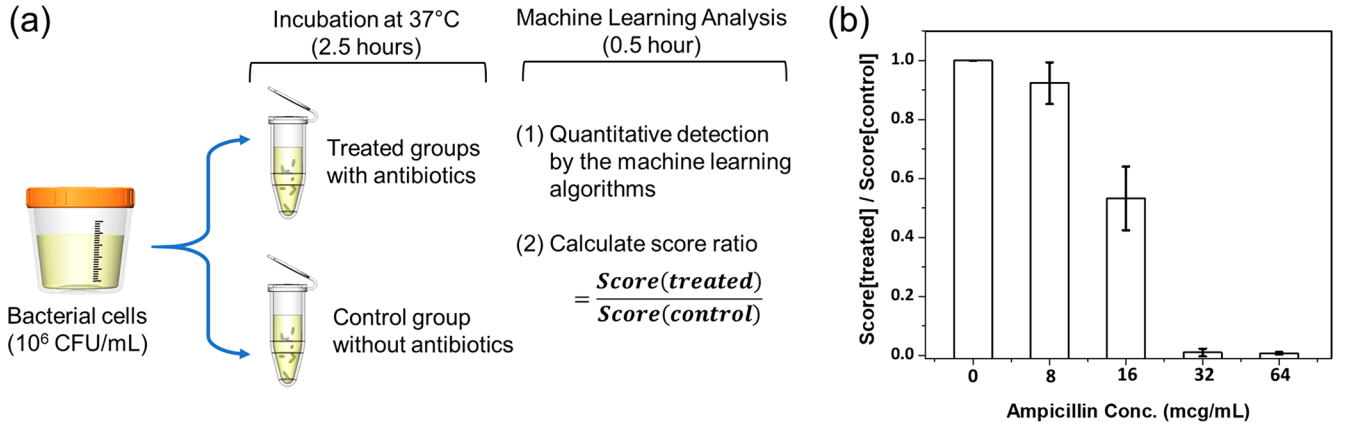

Figure 4. (a) Overview of the phenotypic approach for dose–response testing. The procedures start with the growth of 10^6 CFU bacteria in LB buffer with 0 (control), 8, 16, 32, and 64 μg/mL of ampicillin. All cultured samples are then processed with our protocols for quantification by calculating the score ratio. (b) Ampicillin-susceptible *E. coli* (JM109) were cultured for 2.5 h at different concentration of ampicillin. Phenotypic dose–response relationship is performed by using the molecular agglutination approach for quantification. The samples without ampicillin are used as the control. All sample scores after incubation (t = 2.5 h) are compared with a control sample score to calculate the score ratio. When the score ratio is observed unchanged at an ampicillin concentration higher than a specific value, it indicates *E. coli* cells are susceptible to ampicillin.

test involves two separate steps, namely, the sample preparation step and detection step. This work focuses on presenting novel developments in the detection platform. The sample preparation step in clinical tests will involve the use of centrifuge on the urine samples. Future efforts will integrate existing techniques, including centrifugal devices and microfluidic automation,[41,42] to implement on-chip sample preparation and further simplify the protocols.

Toward Antimicrobial Susceptibility Testing (AST): Quantifying Dose–Response Relationship. The optimal dose of antibiotic use is critical to decide the best strategy for clinical treatment. Genotypic approaches can only detect known resistant genes and do not recognize mutant bacteria.[43,44] For complex infection diseases such as UTIs, a phenotypic approach that cultivates bacteria with and without antibiotics will provide clinicians a thorough understanding of the antibiotics' efficacy. Since our assay can quantify the concentration of bacteria, we further apply our imaging microfluidic cytometry platform to establish the dose–response relationship of ampicillin and ampicillin-susceptible *E. coli* (JM109). It holds potential for the antimicrobial susceptibility testing (AST) applications. The growth-based phenotypic approaches have been undertaken for UTI antibiotic assessment.[45,46] As shown in Figure 4a, in our platform, ampicillin-susceptible *E. coli* (~10^6 CFU) were incubated with ampicillin at different concentrations, including 0, 8, 16, 32, and 64 μg/mL, in Luria broth buffer for 2.5 h, respectively. The quantification of *E. coli* at each ampicillin concentration is calculated with the score ratio of antibiotic-treated to control samples (score[treated]/score[control]). Ampicillin is a bacteriolytic antibiotic for Gram-positive and Gram-negative bacteria.[47] Ampicillin not only inhibits biosynthesis of the bacterial cell wall but eventually lyses bacteria. In the presence of a sufficient ampicillin dose, the *E. coli* cell wall is disrupted, and the target 16S rRNAs are removed during the protocols. The decreasing score ratio is expected. In the clinic, antibiotic susceptibility can be observed by the score ratio change. As shown in Figure 4b, when the antibiotic concentration is higher than 32 μg/mL, the score ratio starts to remain unchanged. It is indicated that the bacterial sample was susceptible to ampicillin at the specific concentration. Our results of ampicillin at 32 μg/mL to inhibit *E. coli* growth is close to the minimum inhibitory concentration (MIC) in the Clinical and Laboratory Standards Institute (CLSI) guideline.[48] We will further apply this approach to bactericidal antibiotics such as ciprofloxacin. The preliminary data demonstrate the capability of our platform to find the optimal dose of antibiotics in less than 3 h from phenotypic cell growth to bacterial growth quantification. The dose–response relationship is an essential step toward AST applications for clinical decision-making.

CONCLUSIONS

We demonstrated a molecular diagnostic approach that uses a pair of nucleotide probes targeting bacterial 16S rRNA to form an agglutination assay. Employing the narrow beam scanning technique on the microfluidic imaging flow cytometer, the molecular agglutination assay can offer a low-cost and high specificity diagnostic platform for rapid pathogen identification of UTIs. Our protocol is no-wash and amplification-free, eliminating possible human error and simplifying diagnostic procedures.

As a proof-of-concept study, we used microparticles coated with probes matching 16S rRNA of specific pathogens. Off-the-shelf CMOS imagers such as smartphone cameras can be used as the readout sensor. Unlike fluorescent labeling techniques, we analyzed scattered light images from agglutinated microparticles. Employing machine learning algorithms, the features of agglutinated patterns can be extracted for quantification of bacterial levels. Therefore, it requires no washing step for background noise removal or signal-to-noise ratio enhancement. The limit of detection in this preliminary study is 10^2 CFU/mL, which is several orders of magnitude below the clinical cutoff for clinical UTI diagnosis. The dynamic range for *E. coli* detection spans 5 orders of magnitude in bacterial concentration (10^2 to 10^7 CFU/mL). The procedure takes less than 30 min from sample preparation to results for pathogen identification. In the rare case where the bacterial concentration is beyond the range of detection, dilutions and multiple measurements would be required to confirm the results. We validated the molecular agglutination assay with 50 UTI patient samples. The trained imaging model

DOI: 10.1021/acscentsci.8b00447
ACS Cent. Sci. 2018, 4, 1485–1494

successfully distinguished all *E. coli* positive samples from clinical samples without false positives. It implies that the proposed protocols can deliver clinically accurate diagnosis and significantly reduce turnaround time. In addition, we also piloted the dose−response testing by leveraging the capability of quantifying the bacterial concentration. The growth-based dose−response testing was performed to examine ampicillin-susceptible *E. coli* strains within 3 h. Our platform clearly observed the effect of ampicillin amount against the growth of *E. coli* by analyzing the score ratio change. This approach demonstrated an essential step toward AST applications and the possibility to shorten the time required to obtain antibiotic treatment guidance.

To conclude, we present a microfluidic imaging flow cytometry platform that provides clinically relevant results for UTI pathogen identification and antibiotic treatment guidance. Given the inexpensive test and readout component cost as well as simple protocols (no fluorescent labeling and washing steps), this platform holds great potential for rapid pathogen diagnostics from the laboratory to POCT settings. Although off-chip protocols were used in this study, we acknowledge more efforts of microfluidic chip integration have to be completed for on-chip bacterial sample handling. Other future work will include system integration of multiplexed pathogen identification assay, on-chip sample preparation, and miniaturization of the system with minimal human intervention, paving the way toward a "sample-in, answer-out" point-of-care testing platform for future clinical uses.

MATERIALS AND METHODS

Materials. Triton X-100 (Sigma-Aldrich), Tris-HCI (1 M, pH 8.0, Invitrogen), EDTA (0.5 M, pH 8.0, Invitrogen), lysozyme from chicken egg white (Sigma-Aldrich), streptavidin conjugated magnetic beads (1 μm, OceanNanoTech), sodium chloride (Sigma-Aldrich), 20× SSC (IBI Scientific), sodium dodecyl sulfate solution (10%, Sigma-Aldrich), UltraPure distilled water (Invitrogen), bovine serum albumin (>98%, Sigma-Aldrich), 1× phosphate buffered saline (Sigma-Aldrich), Biotinylated single-stranded oligonucleotides with C12 linker between biotin and oligonucleotides (Eton Bioscience).

EC1:5′-biotin-C12-CTGCGGGTAACGTCAA-TGAGCAAA-3′

EC2:5′-GGTATTAACTTTACTCCCTTCCTC-C12-biotin-3′.

Reagents. Washing buffer: 10 mM Tris-HCl, 1 mM EDTA, and 2 M NaCl. Storage buffer: 4 mM EDTA, 40 mM Tris−HCl of pH 8.0, and 0.2% Triton X-100. Biotinylated probe molecule solution: suspend dry oligonucleotides in the ultrapure distilled water to normalize the concentration of 10 nmol/mL. Lysis buffer: 15 mg of lysozyme dissolved in 1 mL of storage buffer. Hybridization buffer: 0.5× SSC, 0.1% SDS, and 1% BSA.

Probe-Coating on Magnetic Microparticles. 50 μL suspension is taken from streptavidin conjugated magnetic bead solution (4 mg/mL). Resuspend 50 μL of bead aliquot in the centrifuge tube, followed by placing the tube on a magnet separator for 1 min and discarding the supernatant. Resuspend magnetic beads in 200 μL of washing buffer. Place on the magnet separator and discard supernatant. Repeat washing step twice. Resuspend magnetic beads with 100 μL of washing buffer and mix with 100 μL of biotinylated probe molecule solution. Incubate for 15 min at room temperature with gentle rotation of the tube. Place the tube on the magnet separator and discard the supernatant. Wash the coated beads 2 times with storage buffer. Add 250 μL of storage buffer to resuspend probe-coating magnetic microparticles.

Fabrication of Microfluidic Chips. The design of the microfluidic device can be referred to our previous work.[18] In brief, the microfluidic chip contains an inlet, a serpentine microchannel, a sensing window, a waste collection reservoir, and an outlet. The waste reservoir was designed to hold up to 25 μL of liquid sample. The microfluidic channel width at the entrance is 600 μm and expanded to 900 μm in the sensing window area. The microfluidic device is comprised of (1) base layer: hydrophilic tape (3M 9962) as the material of the microfluidic devices to transport lysate samples without any external pumps, (2) channel layer: a double-sided light shielding tape (Avery Dennison, FT 5250) cut with microfluidic channels, and (3) top layer: hydrophilic tape (3M 9962) for inlet and outlet openings. The microfluidic chips were manufactured by using the production lamination process (LasX Industries Inc., MN).

CMOS Imager-Based Imaging Flow Cytometer. As described in our previous studies, the narrow beam scanning technique leveraged a microfabricated lens to produce the narrow beam for scattered light scanning. The detailed fabrication can be found in ref 19. The smartphone dongle was designed as a housing for a microlens embedded glass slide, an optical lens with effective focal length of 2.51 mm (Largan Precision Co., Taiwan), and an LED. The dongle prototyped using a 3-D printer is optically aligned with the camera on an iPhone 5S (Apple, Cupertino, CA). The detail of smartphone dongle can refer to the Supporting Information, Figure S5. With proper optimization, this mechanical structure can be tailored for other mobile devices such as versatile Android devices as well. Due to strong scattered light from agglutinated microparticles, we converted the low-end CMOS imager to a sensitive biosensing reader.

Patient Samples. Patient urine samples, sent to University of California San Diego hospital for microbiological analysis, were used in this study. Human subject involvement in this study was approved by the University of California, San Diego Administrative Panel on Human Subjects in Medical Research. The study was certified as category 4 exempt, which includes research involving the collection or study of existing data, documents, records, pathological specimens, or diagnostic specimens, if the information is recorded in such a manner that subjects cannot be identified directly or through identifiers linked to the subjects.

Cell Culture. Clinical samples, including *E. coli*, *Citrobacter*, *Klebsiella pneumoniae*, *Proteus mirabilis*, *Enterobacter*, *Morganella morganii*, *Providencia*, and *Pseudomonas aeruginosa*, and *E. coli* lab strain JM109 were applied in the experiment. The clinical samples were collected from different patients with diagnosed UTIs. Some of clinical samples contained more than one bacterial type (refer to Supporting Information, Table S2). When receiving clinical isolates, samples were inoculated with Luria broth (LB) buffer in a shaker at 37 °C at 250 rpm and grown overnight. The grown bacteria were then mixed with 25% glycerol and stored at −80 °C prior to use. Before each experiment, the frozen samples were grown in LB for 8 h and adjusted concentration, which was calibrated with the plate culture and the spectrophotometer.

Detection Protocols. To establish the titration curve of *E. coli* analysis, the overnight cultured (8 h) *E. coli* JM109 bacteria were first measured O.D. to be ∼0.9 (4.5×10^8 CFU/mL),

DOI: 10.1021/acscentsci.8b00447
ACS Cent. Sci. 2018, 4, 1485−1494

and a serial dilution of bacterial samples was performed in phosphate-buffered saline (PBS) buffer to make the bacterial concentration 0 (i.e., negative control), 10^2, 10^3, 10^4, 10^5, 10^6, and 10^7 CFU/mL. To demonstrate our agglutination assay, 1 mL bacterial sample in PBS buffer was centrifuged at 10 000 rpm for 3 min and 980 μL was supernatant meticulously discarded without agitating the bacterial pellet. The 12 μL of lysis buffer was added into bacterial samples with gently pipetting and incubated for 3 min at room temperature. Five microliters of EC1 and EC2 probes was added into lysate, respectively. 68 μL of hybridization buffer was added to make a total volume of 100 μL at pH = 7.2. The mixture was gently vibrated by the vortex and incubated in a water bath incubator for 25 min at 37 °C to initiate the hybridization between the bacterial 16S rRNA and the probe on microparticles. After rigorously agitation, 20 μL of mixture was transferred onto the microfluidic chip inserted in the smartphone dongle. The mixture will be imbibed into microfluidic channel for the NBS interrogation. The flowing agglutination pattern was recorded at 30 fps for 60 s, which is the maximum frame rate supported by the iPhone 5S. Triplicate experiments were conducted for each bacterial level to establish the regression curve for *E. coli*. All images of agglutinated pattern from *E. coli* samples were used for machine learning model training. As for clinical specificity validation, the same protocols and trained model were used. The cost per test is around $0.26 (detail can be found in Supporting Information, Table S3).

Dose−Response Relationship. Ampicillin-susceptible *E. coli* (JM109) bacteria were first calibrated O.D. to be ∼0.8 (4×10^8 CFU/mL) in PBS buffer. ∼4×10^6 CFU of *E. coli* cells were inoculated into 5 mL of LB buffer, containing 0, 8, 16, 32, and 64 μg/mL of ampicillin, respectively. Bacterial samples were incubated at 37 °C for 2.5 h. After incubation, the bacterial samples were used in the same detection protocols for three times at each ampicillin concentration.

Image Processing. The video was recorded using an iPhone 5S at a frame rate of 30 frames per second, and saved in MOV format with a resolution of 1920 × 1080 pixels. The video files were transferred to a laptop, and processed using OpenCV Library.[49] The video consists of image sequence, where each image was converted into hue, saturation, value (HSV) color space. A threshold of upper (H = 0, S = 0, V = 100) and lower (H = 180, S = 255, V = 255) HSV boundary was applied to identify the dark-field imaging band. The Otsu's algorithm was then applied to automatically calculate the optimum thresholding that best separates the scattered light and the background noise in the dark-field imaging band.[50] The agglutinated clusters were identified by Suzuki's chain approximation algorithm.[51]

The pattern of each agglutinated cluster was described by topology and intensity features in the grayscale color space: (1) size, (2) scattered light intensity, (3) circularity, and (4) regularity. The *size* is calculated as the area of the agglutinated cluster. The *scattered light intensity* is calculated as the total intensity of the agglutinated cluster. The *circularity* is calculated as the ratio of the area of the agglutinated cluster to the minimum area of the enclosing circle. The count is calculated by the numbers of agglutinated clusters. The *regularity* is calculated as the ratio of the height to the width of the rotated bounding rectangle enclosing the agglutinated cluster. In addition to the described features of agglutinated cluster, each dark-field imaging band was also described by two features: the size of agglutinated and nonagglutinated area.

Machine Learning. We accumulated features over 50 frames to generalize the agglutination pattern. The sum and the standard deviation of each feature were computed to represent the profile of the accumulated agglutination patterns. In addition, we used the total area of the dark-field imaging band as the normalizing factor in the profile. The profiles were shuffled and split into training and validation sets: 70% of the profiles for training sets and 30% for validation sets. The profiles were then standardized by independently centering and scaling on each feature to unit variance on the samples in the training set. The same scaling parameters were applied to validation set for the testing of the model.

Linear regression, SVM, and neural network model were trained on the standardized agglutination profile using Scikit-learn. We used radial basis function kernel in the SVM model. We applied rectified linear unit (ReLU) activation function to the neural network model and optimized the loss function using Adam stochastic optimization algorithm.[52,53] The exponential decay rates for estimates of the first and second moment vector were set 0.9 and 0.999, respectively. The value for the numerical stability was set to 10^{-8}. We conducted an exhaustive grid search over *L2 penalty* and *initial learning rate* parameters, which were optimized by 10-fold cross-validation in the training set. The score corresponding to the standardized agglutination profile was calculated as the weighted mean of the concentration level c_i in log10 scale:

$$\text{score} = \frac{\sum_i W_i * c_i}{\sum_i W_i}$$

The weight was calculated as the exponential function of weighted linear summation of input features $X = x_1, x_2, ..., x_m$, added to a bias vector, and followed by ReLU activation function:

$$W_i = e^{\max(w * x_m + \text{bias}, 0)}$$

Scoring. Each sample was recorded for 60 s using iPhone 5S as described aforementioned in the Image Processing section. The video file was then transferred to a laptop for imaging processing and scoring. The neural network model returns a score based on the agglutination profile for each sample. The processing time from a raw video file to the answer is completed in 2 min using one core of 2.7 GHz Intel Core i5 (MacBook Pro) or in 5 min using one core of 1.4 GHz ARM (Raspberry Pi 3B).

Safety Statement. No unexpected or unusually high safety hazards were encountered in this work.

■ ASSOCIATED CONTENT

Supporting Information

The Supporting Information is available free of charge on the ACS Publications website at DOI: 10.1021/acscentsci.8b00447.

Additional information regarding algorithms, physical setup of the detection platform, data from clinical samples, and cost per test (PDF)

■ AUTHOR INFORMATION

Corresponding Authors

*(T.-F.W.) E-mail: tfwu@jacobs.ucsd.edu.

*(O.S.P.) E-mail: opak@scu.edu.

DOI: 10.1021/acscentsci.8b00447
ACS Cent. Sci. 2018, 4, 1485−1494

ORCID

Tsung-Feng Wu: 0000-0003-1226-7741

Author Contributions

#T.W. and Y.C. contributed equally to this work. T.W. and Y.C. performed experiments. T.W. and O.P. designed and supervised the study. W.W. and Y.F. designed and prototyped hardware components. S.F. simulated and prototyped microfluidic chips. D.P. provided clinical patient samples and guidance. T.W., Y.C., and O.P. wrote the manuscript.

Funding

The cost of material and corresponding consumables was supported by VOR, Inc.

Notes

The authors declare the following competing financial interest(s): T.W. and Y.C. are cofounders and shareholders of VOR, Inc., which is involved in commercializing the detection platform. All other authors declare no competing interests.

■ ACKNOWLEDGMENTS

We thank Dr. Tsung-I Tsai for the gift of the lab strain *E. coli* (JM109) for this study.

■ REFERENCES

(1) Johnson, J. R. Laboratory diagnosis of urinary tract infections in adult patients. *Clin. Infect. Dis.* **2004**, *39*, 873 author reply 873−874 .

(2) Foxman, B. Urinary Tract Infection Syndromes: Occurrence, Recurrence, Bacteriology, Risk Factors, and Disease Burden. *Infectious Disease Clinics of North America* **2014**, *28*, 1−13.

(3) Schappert, S. M.; Rechtsteiner, E. A. Ambulatory medical care utilization estimates for 2007. *Vital Health Stat.* **2011**, *169*, 1−38.

(4) CDC, Catheter-associated Urinary Tract Infections (CAUTI). https://www.cdc.gov/hai/ca_uti/uti.html.

(5) Magill, S. S.; Edwards, J. R.; Bamberg, W.; Beldavs, Z. G.; Dumyati, G.; Kainer, M. A.; Lynfield, R.; Maloney, M.; McAllister-Hollod, L.; Nadle, J.; Ray, S. M.; Thompson, D. L.; Wilson, L. E.; Fridkin, S. K. Multistate point-prevalence survey of health care-associated infections. *N. Engl. J. Med.* **2014**, *370*, 1198−1208.

(6) CDC, HAI Data and Statistics. https://www.cdc.gov/hai/surveillance/.

(7) Kennedy, E. H.; Greene, M. T.; Saint, S. Estimating hospital costs of catheter-associated urinary tract infection. *J. Hosp Med.* **2013**, *8*, 519−522.

(8) Foxman, B. The epidemiology of urinary tract infection. *Nat. Rev. Urol.* **2010**, *7*, 653−660.

(9) Gupta, K.; Hooton, T. M.; Naber, K. G.; Wullt, B.; Colgan, R.; Miller, L. G.; Moran, G. J.; Nicolle, L. E.; Raz, R.; Schaeffer, A. J.; Soper, D. E. International clinical practice guidelines for the treatment of acute uncomplicated cystitis and pyelonephritis in women: A 2010 update by the Infectious Diseases Society of America and the European Society for Microbiology and Infectious Diseases. *Clin. Infect. Dis.* **2011**, *52*, e103−120.

(10) Zhanel, G. G.; Hisanaga, T. L.; Laing, N. M.; DeCorby, M. R.; Nichol, K. A.; Weshnoweski, B.; Johnson, J.; Noreddin, A.; Low, D. E.; Karlowsky, J. A.; Hoban, D. J. Antibiotic resistance in *Escherichia coli* outpatient urinary isolates: final results from the North American Urinary Tract Infection Collaborative Alliance (NAUTICA). *Int. J. Antimicrob. Agents* **2006**, *27*, 468−475.

(11) Davenport, M.; Mach, K. E.; Shortliffe, L. M. D.; Banaei, N.; Wang, T. H.; Liao, J. C. New and developing diagnostic technologies for urinary tract infections. *Nat. Rev. Urol.* **2017**, *14*, 296−310.

(12) Drain, P. K.; Hyle, E. P.; Noubary, F.; Freedberg, K. A.; Wilson, D.; Bishai, W. R.; Rodriguez, W.; Bassett, I. V. Diagnostic point-of-care tests in resource-limited settings. *Lancet Infect. Dis.* **2014**, *14*, 239−249.

(13) Gong, M. M.; MacDonald, B. D.; Nguyen, T. V.; Van Nguyen, K.; Sinton, D. Lab-in-a-pen: a diagnostics format familiar to patients for low-resource settings. *Lab Chip* **2014**, *14*, 957−963.

(14) van der Zee, A.; Roorda, L.; Bosman, G.; Ossewaarde, J. M. Molecular Diagnosis of Urinary Tract Infections by Semi-Quantitative Detection of Uropathogens in a Routine Clinical Hospital Setting. *PLoS One* **2016**, *11*, e0150755.

(15) Burillo, A.; Rodriguez-Sanchez, B.; Ramiro, A.; Cercenado, E.; Rodriguez-Creixems, M.; Bouza, E. Gram-stain plus MALDI-TOF MS (Matrix-Assisted Laser Desorption Ionization-Time of Flight Mass Spectrometry) for a rapid diagnosis of urinary tract infection. *PLoS One* **2014**, *9*, e86915.

(16) Priye, A.; Bird, S. W.; Light, Y. K.; Ball, C. S.; Negrete, O. A.; Meagher, R. J. A smartphone-based diagnostic platform for rapid detection of Zika, chikungunya, and dengue viruses. *Sci. Rep.* **2017**, *7*, 44778.

(17) Wei, Q.; Qi, H.; Luo, W.; Tseng, D.; Ki, S. J.; Wan, Z.; Gorocs, Z.; Bentolila, L. A.; Wu, T. T.; Sun, R.; Ozcan, A. Fluorescent imaging of single nanoparticles and viruses on a smart phone. *ACS Nano* **2013**, *7*, 9147−9155.

(18) Wu, T.-F.; Chen, Y.-C.; Wang, W.-C.; Kucknoor, A. S.; Lin, C.-J.; Lo, Y.-H.; Yao, C.-W.; Lian, I. Rapid Waterborne Pathogen Detection with Mobile Electronics. *Sensors* **2017**, *17*, 1348.

(19) Wu, T. F.; Yen, T. M.; Han, Y.; Chiu, Y. J.; Lin, E. Y.; Lo, Y. H. A light-sheet microscope compatible with mobile devices for label-free intracellular imaging and biosensing. *Lab Chip* **2014**, *14*, 3341−3348.

(20) Chunara, R.; Godin, M.; Knudsen, S. M.; Manalis, S. R. Mass-based readout for agglutination assays. *Appl. Phys. Lett.* **2007**, *91*, 193902.

(21) Uddin, R.; Burger, R.; Donolato, M.; Fock, J.; Creagh, M.; Hansen, M. F.; Boisen, A. Lab-on-a-disc agglutination assay for protein detection by optomagnetic readout and optical imaging using nano- and micro-sized magnetic beads. *Biosens. Bioelectron.* **2016**, *85*, 351−357.

(22) Mezger, A.; Fock, J.; Antunes, P.; Osterberg, F. W.; Boisen, A.; Nilsson, M.; Hansen, M. F.; Ahlford, A.; Donolato, M. Scalable DNA-Based Magnetic Nanoparticle Agglutination Assay for Bacterial Detection in Patient Samples. *ACS Nano* **2015**, *9*, 7374−7382.

(23) Tsai, C. T.; Robinson, P. V.; Spencer, C. A.; Bertozzi, C. R. Ultrasensitive Antibody Detection by Agglutination-PCR (ADAP). *ACS Cent. Sci.* **2016**, *2*, 139−147.

(24) Cho, S.; Park, T. S.; Nahapetian, T. G.; Yoon, J. Y. Smartphone-based, sensitive microPAD detection of urinary tract infection and gonorrhea. *Biosens. Bioelectron.* **2015**, *74*, 601−611.

(25) Antunes, P.; Watterson, D.; Parmvi, M.; Burger, R.; Boisen, A.; Young, P.; Cooper, M. A.; Hansen, M. F.; Ranzoni, A.; Donolato, M. Quantification of NS1 dengue biomarker in serum via optomagnetic nanocluster detection. *Sci. Rep.* **2015**, *5*, 16145.

(26) Vollenhofer-Schrumpf, S.; Buresch, R.; Schinkinger, M. A simple nucleic acid hybridization/latex agglutination assay for the rapid detection of polymerase chain reaction amplicons. *J. Microbiol. Methods* **2007**, *68*, 568−576.

(27) Ihara, T.; Tanaka, S.; Chikaura, Y.; Jyo, A. Preparation of DNA-modified nanoparticles and preliminary study for colorimetric SNP analysis using their selective aggregations. *Nucleic Acids Res.* **2004**, *32*, e105.

(28) Storhoff, J. J.; Elghanian, R.; Mucic, R. C.; Mirkin, C. A.; Letsinger, R. L. One-Pot Colorimetric Differentiation of Polynucleotides with Single Base Imperfections Using Gold Nanoparticle Probes. *J. Am. Chem. Soc.* **1998**, *120*, 1959−1964.

(29) DeLong, E. F.; Wickham, G. S.; Pace, N. R. Phylogenetic stains: ribosomal RNA-based probes for the identification of single cells. *Science* **1989**, *243*, 1360−1363.

(30) Riahi, R.; Mach, K. E.; Mohan, R.; Liao, J. C.; Wong, P. K. Molecular detection of bacterial pathogens using microparticle enhanced double-stranded DNA probes. *Anal. Chem.* **2011**, *83*, 6349−6354.

DOI: 10.1021/acscentsci.8b00447
ACS Cent. Sci. 2018, 4, 1485−1494

(31) Switz, N. A.; D'Ambrosio, M. V.; Fletcher, D. A. Low-cost mobile phone microscopy with a reversed mobile phone camera lens. *PLoS One* **2014**, *9*, e95330.
(32) Ephraim, R. K.; Duah, E.; Cybulski, J. S.; Prakash, M.; D'Ambrosio, M. V.; Fletcher, D. A.; Keiser, J.; Andrews, J. R.; Bogoch, II. Diagnosis of Schistosoma haematobium infection with a mobile phone-mounted Foldscope and a reversed-lens CellScope in Ghana. *Am. J. Trop. Med. Hyg.* **2015**, *92*, 1253−1256.
(33) Gao, Y.; Wolf, L. K.; Georgiadis, R. M. Secondary structure effects on DNA hybridization kinetics: a solution versus surface comparison. *Nucleic Acids Res.* **2006**, *34*, 3370−3377.
(34) Wiklund, M.; Nord, O.; Gothall, R.; Chernyshev, A. V.; Nygren, P. A.; Hertz, H. M. Fluorescence-microscopy-based image analysis for analyte-dependent particle doublet detection in a single-step immunoagglutination assay. *Anal. Biochem.* **2005**, *338*, 90−101.
(35) Amarasiri Fernando, S.; Wilson, G. S. Studies of the 'hook' effect in the one-step sandwich immunoassay. *J. Immunol. Methods* **1992**, *151*, 47−66.
(36) Kass, E. H. Bacteriuria and the diagnosis of infections of the urinary tract: With observations on the use of methionine as a urinary antiseptic. *A.M.A. Archives of Internal Medicine* **1957**, *100*, 709−714.
(37) Kass, E. H. Pyelonephritis and bacteriuria: A major problem in preventive medicine. *Ann. Intern. Med.* **1962**, *56*, 46−53.
(38) Nicolle, L. E.; Bradley, S.; Colgan, R.; Rice, J. C.; Schaeffer, A.; Hooton, T. M. Infectious Diseases Society of America Guidelines for the Diagnosis and Treatment of Asymptomatic Bacteriuria in Adults. *Clin. Infect. Dis.* **2005**, *40*, 643−654.
(39) Chang, C.-C.; Lin, C.-J. LIBSVM: A library for support vector machines. *ACM Trans. Intell. Syst. Technol.* **2011**, *2*, 1−27.
(40) Chang, Y.-W.; Hsieh, C.-J.; Chang, K.-W.; Ringgaard, M.; Lin, C.-J. Training and Testing Low-degree Polynomial Data Mappings via Linear SVM. *J. Mach. Learn. Res.* **2010**, *11*, 1471−1490.
(41) Boardman, A. K.; Campbell, J.; Wirz, H.; Sharon, A.; Sauer-Budge, A. F. Rapid microbial sample preparation from blood using a novel concentration device. *PLoS One* **2015**, *10*, e0116837.
(42) Song, J.; Liu, C.; Mauk, M. G.; Rankin, S. C.; Lok, J. B.; Greenberg, R. M.; Bau, H. H. Two-Stage Isothermal Enzymatic Amplification for Concurrent Multiplex Molecular Detection. *Clin. Chem.* **2017**, *63*, 714−722.
(43) Walsh, C. Molecular mechanisms that confer antibacterial drug resistance. *Nature* **2000**, *406*, 775.
(44) Cirz, R. T.; Chin, J. K.; Andes, D. R.; de Crecy-Lagard, V.; Craig, W. A.; Romesberg, F. E. Inhibition of mutation and combating the evolution of antibiotic resistance. *PLoS Biol.* **2005**, *3*, e176.
(45) Athamanolap, P.; Hsieh, K.; Chen, L.; Yang, S.; Wang, T. H. Integrated Bacterial Identification and Antimicrobial Susceptibility Testing Using PCR and High-Resolution Melt. *Anal. Chem.* **2017**, *89*, 11529−11536.
(46) Avesar, J.; Rosenfeld, D.; Truman-Rosentsvit, M.; Ben-Arye, T.; Geffen, Y.; Bercovici, M.; Levenberg, S. Rapid phenotypic antimicrobial susceptibility testing using nanoliter arrays. *Proc. Natl. Acad. Sci. U. S. A.* **2017**, *114*, E5787−E5795.
(47) Sorg, R. A.; Veening, J.-W. Microscale insights into pneumococcal antibiotic mutant selection windows. *Nat. Commun.* **2015**, *6*, 8773.
(48) *Development of in Vitro Susceptibility Testing Criteria and Quality Control Parameters*; CLSI guideline M23, 4th ed.; Clinical and Laboratory Standards Institute: Wayne, PA, 2016.
(49) Kaehler, A.; Bradski, G. *Learning OpenCV 3: Computer Vision in C++ with the OpenCV Library*; O'Reilly Media, 2016.
(50) Sezgin, M.; Sankur, B. In *Tilte*; SPIE, 2004.
(51) Suzuki, S.; be, K. Topological structural analysis of digitized binary images by border following. *Computer Vision, Graphics, and Image Processing* **1985**, *30*, 32−46.
(52) Nair, V.; Hinton, G. E. Rectified linear units improve restricted Boltzmann machines. In *Proceedings of the 27th International Conference on International Conference on Machine Learning*; Omnipress: Haifa, Israel, 2010; pp 807−814.
(53) Wu, T. F.; Mei, Z.; Lo, Y. H. Label-free Optofluidic Cell Classifier Utilizing Support Vector Machines. *Sens. Actuators, B* **2013**, *186*, 327−332.

DOI: 10.1021/acscentsci.8b00447
ACS Cent. Sci. 2018, 4, 1485−1494